Non-aliphatic Protic Ammonia for Post Healing of Formamidinium-containing Perovskite Films

Shuping Pang (pangsp@qibebt.ac.cn)
Qingdao Institute of Bioenergy and Bioprocess Technology, Chinese Academy of Sciences
https://orcid.org/0000-0002-2526-4104

Zhipeng Li
Qingdao Institute of Bioenergy and Bioprocess Technology, Chinese Academy of Sciences

Xiao Wang
Qingdao Institute of Bioenergy and Bioprocess Technology, Chinese Academy of Sciences

Zaiwei Wang
École Polytechnique Fédérale de Lausanne https://orcid.org/0000-0001-9725-0206

Zhipeng Shao
Qingdao Institute of Bioenergy and Bioprocess Technology, Chinese Academy of Sciences

Lianzheng Hao
Qingdao Institute of Bioenergy and Bioprocess Technology, Chinese Academy of Sciences

Xiaofan Du
Qingdao Institute of Bioenergy and Bioprocess Technology, Chinese Academy of Sciences

Yi Rao
Qingdao Institute of Bioenergy and Bioprocess Technology, Chinese Academy of Sciences

Chen Chen
Qingdao Institute of Bioenergy and Bioprocess Technology, Chinese Academy of Sciences

Dachang Liu
Qingdao Institute of Bioenergy and Bioprocess Technology, Chinese Academy of Sciences

Li Wang
Qingdao Institute of Bioenergy and Bioprocess Technology, Chinese Academy of Sciences

Guanglei Cui
Qingdao Institute of Bioenergy and Bioprocess Technology, Chinese Academy of Sciences

---

Physical Sciences - Article

Keywords: Gas post healing technology, FA-perovskite materials, Perovskite solar modules, Addition-elimination reaction

Posted Date: January 13th, 2021

DOI: https://doi.org/10.21203/rs.3.rs-139785/v1

Version of Record: A version of this preprint was published at Nature Communications on July 29th, 2022. See the published version at https://doi.org/10.1038/s41467-022-32047-z.

Abstract

The solvents employed for perovskite materials not only play roles in dissolving the precursors but also participate in crystallization process. The high boiling point aprotic solvents with O-donor coordinating ligands have been extensively studied, but a highly uniform film still requires the participation of additives or an additional step to accelerate the nucle-ation rate. The volatile protic aliphatic amines with both coordinating ligands and hydrogen proton facilitate the pro-cessing of pure MAPbX3 perovskite films with higher crystallinity, fewer defects, and easier for large scale fabrication as well. However, their attempts in FA-containing perovskite is challenged heretofore. Here, the degradation mechanism of FA-containing perovskite in aliphatic amines environment has been revealed, and non-aliphatic ammonia was selected to avoid undesired side reactions. In particular, low temperature is proved to be crucial to enable FAPbI3 perovskite material absorb enough NH3 molecules to form a flowable intermediate state, which is the heart for defect healing. As a result, a rough FA-containing perovskite film was effectively healed to a highly uniform, compact one, toward an efficiency of 23.3% with excellent reproducibility. The manipulating of the interaction between perovskite and ammonia opens up a new di-rection for upscaling the fabrication of highly efficient FA-containing perovskite solar cells.

Main Text

Organic-inorganic hybrid halide perovskite materials with the general formula ABX_3, where A is methylammonium (MA) or formamidinium (FA), B is Pb or Sn, and X is I, Br or Cl, have emerged as a class of promising light-harvesting materials since 2009[1], reaching a certified power conversion efficiencies (PCE) as high as 25.5%[2], which is comparable to commercialized thin-film solar cell technologies. The crystal structure of ABX_3 perovskite can be regarded as a $[MX_6]^{4-}$ octahedron in a three-dimensional (3D) space with a common apex angle connecting, where the A site ions fill up the gap of the octahedral and the structure is stabilized by Van der Waals forces[3]. These special structural characteristics provide us with a variety of solution processing methods to prepare high-quality perovskite films[4-6].

The high boiling point polar dimethylformamide (DMF), γ-butyrolactone (GBL), dimethyl sulfoxide (DMSO) and N,N-dimethylacetamide (DMA) are the common solvents employed to dissolve the perovskite precursors with the forming of solvated iodoplumbate complexes related to the coordination between O-donor ligands (OL) and Pb(II)[4, 7-9]. The Lewis basicity of solvents is thought to correlate with “coordinating ability” with lead halide salt which can be predicted by their Gutmann’s Donor Number (D_N) with a trend of DMSO>DMA>DMF>GBL[10-11]. The higher D_N solvents coordinate more strongly with the Pb(II) center, which in turn results in the formation of intermediate OL-PbI_2-RAI (R refers to MA or FA, etc.) prior to perovskite crystallization during the film fabrication process. The anisotropic growth nature of the intermediate phase leads to one-dimensional (1D) fiber-like structures[12]. In this regard, it is definitely efficacious to introduce stronger coordinating additives (such as Thiourea[13] and Pyridine[14]) and the fast nucleation scenarios (such as antisolvent extraction, gas-quenching, and vacuum-assisted drying) to modify the crystal nucleation/growth nature of the intermediate phase[7, 15-16].

Among of them, the polar protic aliphatic methylamine gas (MA^g) featured with the presence of hydrogen bonding and low boiling point is becoming an impressive coordinating agent to regulate the crystallization process of thin pure $MAPbI_3$ films[17-19]. In this case, the formed intermediate is a novel metastable (PbI_2-MAI)·xMA complex, instead of simple coordinating bound dominated OL-PbI_2-MAI adduct. The perfect conversion from intermediate (PbI_2-MAI)·xMA to perovskite phase is guaranteed by the disordered nature of hydrogen bonds in (PbI_2-MAI)·xMA intermediate phase and the ultrafast evaporation of MA^g. This healing behavior of MA^g on $MAPbI_3$ perovskite film is firstly reported by Zhou et al. in 2015[18], and the adoption of MA^g as a volatile solvent system has become a commercially viable technology for the $MAPbI_3$ devices with excellent device reproducibility[20-29]. In comparison with MA-rich perovskite films, formamidinium lead iodide ($FAPbI_3$) has more complex crystallization behavior with narrow processing window, which makes it more difficult to achieve the high-quality layers through the normal slot-die coating and spraying technologies. There are already many attempts to introduce MA^g-related methods for the fabrication of FA-based perovskite layer, unfortunately, resulting in degradation of the 3D perovskite phase[21]. The underlying reason of the irreversible transformation of $FAPbI_3$ with protic aliphatic amines treatment is still not fully clear, let alone make efforts to solve this problem.

Here, we have systematically studied the underlying chemical reactions between amines (R-NH_2)/FA gases and MAI/FAI salts used in perovskite precursor under different conditions, and elucidated the condensation reaction between FAI and protic aliphatic amines. On the bases of the interaction of solvent-solute and solute-solute, protic non-aliphatic ammonia (NH_3) was selected to avoid the degradation of the perovskite phase during the post healing process. Particularly, it is demonstrated that low processing temperature is crucial for perovskite layer to enhance NH_3 molecules uptake reaching a flowable state, and the presence of hydrogen bonding enable a homogenous crystallization to pure perovskite phase. As a result, a rough FA-containing perovskite film was effectively healed to a highly uniform, compact one, reaching an efficiency of 23.3%. This demonstrates the high advantage of the NH_3 gas post healing technology, and it is easy for industrial transition for upscaling the fabrication of highly efficient perovskite solar cells.

We started with the study of the underlying chemical reactions between R-NH_2/FA gases and FAI salts (Table 1). The gases involved included methylamine (MA^g), ethylamine (EA^g), propylamine (PA^g), butylamine (BA^g), formamidine (FA^g), and ammonia (NH_3). The preparation of relevant gases and the details of experimental operation are provided in the supporting information. Among of them, the synthesis of pure FA^g is extremely tricky because of its instability at room temperature (RT), which is decisive for its storage and healing treatment for FA-based perovskite films.

First, deuterated DMSO (DMSO-d_6) solvent was used to collect FA^g gas as illustrated in Figure S1(A), where mixed FACl and NaOH powders were kept at RT. The use of DMSO-d_6 is to facilitate subsequent direct nuclear magnetic resonance (NMR) measurement. Unfortunately, only NH_3 signal was detected in

the NMR spectrum (Table1(No.1) and Figure S2). The possible reason is that the boiling point of FA^g is too high to diffuse into the DMSO-d_6 solvent. The formation of the NH_3 is indicative of side reactions in the process of gas preparation (Scheme S1). Then the temperature of the reactor and the gas pipeline was increased to 150 ℃ and DMSO-d_6 solvent was still kept at RT. In this case, four main compounds were detected as follows: s-triazine > formamide > FA > NH_3 (Table1(No.2) and Figure S3). The s-triazine with a boiling point of 114 ℃ should be the product of condensation reaction of three FA molecules with formation of NH_3 (Scheme S1(b)). In comparison, the relatively low NH_3 content is owing to its volatile property and most of NH_3 molecules were evaporated from DMSO-d_6 solution before NMR characterization. This side reaction was also detected when the FAI powder sample was heated at 150 ℃[30]. The by-product formamide should be the hydrolyzation product of FA^g in the presence of H_2O which was generated from the neutralization between the FACl and NaOH (Scheme S1(a)).

Considering that there is long time interval from gas collection to NMR measurement, then acetic acid (HOAc) was employed to capture FA^g. By this way, the as-prepared FA^g could be quickly converted to FAAc before their condensation reaction. As expected, NMR spectrum of the reaction product is exactly FAAc without any other impurity components (Table1(No.3) and Figure S4). The above results strongly indicate that FA^g molecule could be produced, but it only stable in a short time.

Based on this method, the interaction between FAI and FA^g was further studied. The FAI powder was then adopted to capture the as-produced FA^g prepared from FACl and NaOH at 150 ℃. Besides the FAI, there is also formamide signal in the NMR spectrum (Table 1(No.4), Figure S5 and Scheme S1(a)). Now it's clear that the spontaneous decomposition and addition-elimination reaction among the FA^g molecules highly limited their healing effect on $FAPbI_3$ perovskite films.

Table 1. The synthesis of FA^g and chemical reactions between amines/formamidine gases and FAI salts

No.	Gas generation	Gas collection	^{1}H NMR result[a]
1	FACl, NaOH, RT	DMSO-d_6	NH_3
2	FACl, NaOH, 150 ℃	DMSO-d_6	s-triazine, formamide, FA, NH_3[b]
3	FACl, NaOH, 150 ℃	HOAc	FAAc[b]
4	FACl, NaOH, 150 ℃	FAI powder	FAI, formamide
5	MA in EtOH, 60 ℃	FAI powder	DMFAI[b]
6	EACl, NaOH, 60 ℃	FAI powder	DEFAI[b]
7	PA, 60 ℃	FAI powder	DPFAI[b]
8	BA, 60 ℃	FAI powder	DBFAI[b]
9	NH_4OH, RT	FAI powder	NH_4I[b]
10	MA in EtOH/H_2O, 60 ℃	FAI powder	MAI[b]
11	EA in H_2O, 60 ℃	FAI powder	EAI[b]
12	H_2O, 60 ℃	FAI powder	FAI[b]
13	NH_3, RT	FAI powder	FAI[b]

[a] The main components were listed. [b] The sample was dealt with vacuum process to remove low b.p. components. DMFAI is N,N'-dimethyl formamidinium iodide, DEFAI is N,N'- diethyl formamidinium iodide, DPFAI is N,N'- dipropyl formamidinium iodide, and DBFAI is N,N'- dibutyl formamidinium iodide.

Scheme 1. (see Supplementary Files) The addition-elimination reaction and the ion exchange reaction between FAI and R-NH_2 molecules (R is referred to H, Me, Et, n-Pr or n-Bu etc.), and the hydrolysis reaction of FA, RFA and DRFA.

In comparison with FA[g], other amines are much more stable. When FAI powder was treated with MA[g], EA[g], PA[g] and BA[g], the powder firstly transformed to a liquid state, and then the powder was put in vacuum to degas and obtain the final powder (Figure S1B). It is worth noting that there is no FAI signal in NMR spectrum of the final powder sample (Table 1 (No.5-8) and Figure S6).

Taking MA[g] as an example (Table 1(No.5)), the signals founded in NMR spectrum belong to N-methyl formamidinium iodide (MFAI) and N,N'-dimethyl formamidinium iodide (DMFAI) with the mole ratio of about 6:1 (Figure S6(a)). The related chemical reaction mechanism is illustrated in Scheme 1. The MA[g] molecule is nucleophilic and the lone-pair electrons of N atom could attack electrophilic group imine bond in FAI to form MFAI with an addition-elimination process. There is also an imine bond in the formed MFAI, which can carry out the second time addition-elimination reaction with MA[g] to form DMFAI[31]. Meanwhile, ion exchange reactions between FAI, MFAI or DMFAI with MA will also occur, and FA[g], MFA[g] and DMFA[g] will be generated, respectively. In the whole reaction process, the addition-elimination reaction is

irreversible, while the ion exchange reaction is reversible. In the condition with excessive MA^g, the final solid powder is mainly composed of DMFAI.

Similarly, when FAI powder was treated with EA^g, PA^g and BA^g gases, the addition-elimination reaction, ion exchange reaction and the main reaction product are presented in Scheme 1 and Table 1(No. 6-8). It should be also stressed in particular that the above chemical reaction mechanism is only applicable to dry condition. When the gas resource contains H_2O molecules (Figure S1C), the final product is RAI powder rather than RFAI and DRFAI when FAI powder was treated by RA (R is referred to H, Me, Et etc.) gas formed from its aqueous solution. (Table 1 (No. 9-11) and Figure S7). If the FAI powder was treated only by H_2O, there is no other by-products detected in the final product (Table 1 (No.12) and Figure S8). It is speculated that the water molecules can decompose the deprotonated RFA and DRFA to RA and HCOOH (Scheme 1). In comparison, the optical photos and XRD patterns of δ-$FAPbI_3$, $MFAPbI_3$, $DMFAPbI_3$ films, and the α-$FAPbI_3$ films before and after MA^g healing treatment were shown in Figure S9. As we can see, except α-$FAPbI_3$, the other films are all non-perovskite phases. Conceivably, it is because the size of RFA and DRFA cations (R refer to alkyl moiety in MA, EA, PA and BA) are too large to fill the gap of PbI_6 octahedrons for the formation of a stable 3D perovskite phase. This is why aliphatic amines cannot be employed as the solvents or healing gases for fabrication of FA-containing perovskite materials.

Inspired by the above addition-elimination reaction, dry protic NH_3 gas was selected to avoid changes in composition after the gas treatment. As expected, there is no composition change of FAI powder after treating with dry NH_3 gas (Table 1(No.13) and Figure S10) and the corresponding reaction process is presented in Scheme 2. The addition-elimination reaction will still occur, but the actual composition of the FAI powder will not change. Moreover, the H_2O should be avoided during the NH_3 gas treating because it will cause the decomposition of FAI to NH_4I (Figure S7).

Scheme 2. (see Supplementary Files) The reaction between FAI and NH_3 molecules without change in the composition.

The kinetic process of adsorption and desorption of MA/NH_3 gases by MAI/FAI powders was further investigated at RT as shown in Figure 1, which is equally important to evaluate their healing behavior. Started with relatively simple MAI-MA pair, as well known, MAI powder was quickly transformed into a liquid state in the MA gas environment. The MAI·xMA complex was weighed during the process. The whole process is divided into gas absorption (Stage I), degassing at 20 ℃ (Stage II) and degassing at 80 ℃ (Stage III) as illustrated in Figure 1. The MA gas absorption process took place very quickly and reached a saturated state with x value of 2.5 in MAI·xMA (the x value is very sensitive to the temperature and pressure). Once the liquid stated MAI·xMA complex was removed away from MA gas environment, the degassing process happened spontaneously till a relative stable semi-solid state with x value of about 1.1, which is denoted as stage II. When the sample is further heated to 80 ℃ for 10 min (Stage III), the obtained white powder sample with the weight is exactly the same as the raw MAI powder, which

means this is only a simple adsorption and desorption process without any change of chemical constituents before and after reaction between MAI and MA^g. As for the interaction between FAI powder and MA^g, the Stage I and Stage II are similar with MAI-MA pair, but the powder weight cannot return back to its initial value because the formation of MFAI and DMFAI as presented in Scheme 1.

When it comes to the FAI-NH_3 pair, FAI powder also has a rapid NH_3 gas intaking rate to achieve a liquid phase FAI·xNH_3 (Figure S11) with x calculated 3.0 approximately (Stage I). Similar with the interaction between MAI powder and MA^g molecules, the intermediate state FAI·xNH_3 with x ~ 1.3 is ice-like transparent solid state and its XRD pattern is shown in Figure S12. The following thermal annealing at 80 ℃ could fully remove the absorbed NH_3 molecules and obtain the constant weight FAI powder. This phenomenon preliminarily indicates the feasibility of non-aliphatic protic NH_3 to serve as a healing gas for FA-based perovskite films.

NH_3, serving as a healing gas, should have favorable solubility for the FA-based perovskite precursors, including PbI_2 and FAI powder. When the mixed PbI_2/FAI powder was placed in NH_3 gas environment, as shown in Figure 2A, the color of the powder becomes lighter quickly, which is owing to the decreasing of n value in PbI_{2-n} complexes in the sample when coordinated with more and more NH_3 molecules[32]. The coordination bond driven gas intaking is scant and cannot make the (PbI_2-FAI)·xNH_3 into a liquid phase, which is similar to the solid state intermediate phase FAI-PbI_2-DMF and FAI-PbI_2-DMSO. At 20 ℃, the absorbed NH_3 molecules number per $FAPbI_3$ is ~4. It is unexpected that $FAPbI_3$·4NH_3 is still a solid state instead of a liquid state, which is very different from liquid $MAPbI_3$·xMA with x of only 3[29]. One reasonable reason is much smaller size of NH_3 than the MA molecules.

Here the question is how to enhance the x value in $FAPbI_3$·xNH_3. We found that the absorbed amount of NH_3 molecules is seriously associated with the processing temperature. When the temperature was reduced to -5 ℃, a white powder was formed with the x value of ~7. When the temperature was reduced to -15 ℃, the white solid gradually becomes slurry with certain fluidity as presented in right vial of Figure 3A. It was calculated that the x value is ~12 in the liquid state.

The kinetic process of degassing NH_3 gas from $FAPbI_3$·xNH_3 complex was measured in detail by monitoring its weight change when it was kept in an open condition. The degassed NH_3 number per $FAPbI_3$ as the function of time is illustrated in Figure 2B with the temperature increased step-by-step from 20 ℃ to 120 ℃. When we placed the glass vial containing the $FAPbI_3$·xNH_3 slurry on a balance and opened its lid, its weight dropped rapidly at initial stage and then gradually became slower. After 30 min and 60 min, the sample was heated to 40 ℃ and 60 ℃, and maintained for 30 min, respectively. The sample was weighed at regular intervals, showing continuous slow weight loss. When the sample was heated to 80 ℃, the sample quickly reached a relatively stable state then almost no weight change in the

maintaining 30 min, which was calculated about 1 NH_3 molecule per $FAPbI_3$. Finally, the temperature was increased to 120 ℃, the x value is closed to 0, which means that all absorbed NH_3 molecules have been removed without any residue.

The chemical interactions between $FAPbI_3$ and NH_3 molecules were calculated with density functional theory (DFT) method as presented in Figure 2C. As a Lewis base, NH_3 is a coordinating molecule with D_N number (Gutmann's donor number) of 59 Kcal/mol[33], which is strong enough to be as an electron donor with the formation of strong coordination bond with Pb^{2+}. Therefore, the adsorption of one molecule of NH_3 to form $FAPbI_3.1NH_3$ should be owing to the strong coordination bond. In addition to coordination bond, there is the presence of hydrogen bonding, which is necessary for the formation of liquid $FAPbI_3{\cdot}xNH_3$ adduct. The N atom is electronegative because of the presence of lone pair of electrons, which has certain interaction with H atom of FA cations or other NH_3 molecules. It is worth emphasizing that the NH_3 amount absorbed by $FAPbI_3$ is highly related to the temperature and pressure, and here we only calculated the adsorption of 6 NH_3 molecules. It was calculated that there are three different kinds of hydrogen bond lengths between 1 $FAPbI_3$ and 6 NH_3 molecules, 1.73 Å, 2.13 Å, 2.70 Å, respectively. It was also found that the existence of I^- could also form weak hydrogen bond with NH_3 and shorten the hydrogen bond lengths surrounding it (Figure 2C). Therefore, it can be concluded that, in the liquid $FAPbI_3{\cdot}xNH_3$ adduct, there is relatively strong coordination bond between Pb^{2+} and NH_3, medium strength hydrogen bond between FA^+ and NH_3, and much weak hydrogen bond between NH_3 and NH_3 (Figure 2D).

In terms of device fabrication, cesium (Cs) doped $FAPbI_3$ material system was selected to eliminate the formation of the undesired δ-$FAPbI_3$[7]. Firstly, $FA_{0.9}Cs_{0.1}PbI_3$ ($FACsPbI_3$) raw film was deposited on an FTO substrate and then heated at 140 ℃ for 20 min to remove the solvent. The film morphology is shown in scanning electron microscope (SEM) image in Figure 3A with a dull surface. The growth of dendrite-like perovskite crystals, and voids between them is typical of one-step-processed perovskite films using DMF solvent. The size of voids in the starting raw film can reach up to several micrometers. Then the film was transferred into a home-made chamber with a semiconductor chilling plate controlling chamber temperature at -15 ℃. Subsequently, NH_3 gas was introduced into the chamber and the film bleached promptly, with the formation of a colorless intermediate liquid phase $FACsPbI_3{\cdot}xNH_3$. Once removed from the NH_3 gas atmosphere, the film was quickly transferred on a hot plate and heated at 140 ℃ for 20 min. Instead, the dull film changed to a shiny film. All the dendrite-like crystals and voids totally disappeared, and a dense, smooth FA-based perovskite film emerged as displayed in Figure 3B, which is responsible for the visual evolution of film from dull to shiny. It is worth noting that the NH_3 gas absorption and degassing rate of perovskite films take place much faster than powder samples because of their thin thickness. The corresponding atomic force microscope (AFM) image indicated that NH_3 healed perovskite film has a root mean square (RMS) roughness of only 9 nm over a 20 × 20 μm^2 area (Figure 3C), which is lower than the film prepared by the traditional antisolvent method with an RMS of 24 nm (Figure S13).

Figure 3D showed X-ray diffraction (XRD) patterns of spin-coated $FACsPbI_3$ and NH_3 healed $FACsPbI_3$ perovskite films on FTO substrates. After NH_3 gas healing, the diffraction peak intensity of the pure phase (110) preferred orientation perovskite film has increased by more than 100 times. The enhancement of crystallization was also evidenced by a decreased full width at half-maximum (FWHM) of the (110) peaks from 0.203 to 0.114 as compared in Figure 3E. Figure 3F demonstrated ultraviolet-visible (UV-vis) optical absorption and normalized photoluminescence (PL) spectra. Both the raw and healed $FACsPbI_3$ perovskite films presented the same absorption edge at around 815 nm, but NH_3 healed $FACsPbI_3$ perovskite film exhibited significantly increased absorbance in short wavelength region because of the improved film quality and uniformity. The slight blue shift of the PL peak of healed $FACsPbI_3$ perovskite film is attributed to the reduction of shallow level defects as have been previously reported by performing surface passivation[34, 35].

Based on NH_3 gas healing method, $FACsPbI_3$ perovskite films were prepared and studied as the light absorber layers in normal structured perovskite solar cells with SnO_2 as electron transport layer and Spiro-OMeTAD as hole transport layer, respectively. The champion solar cell (Figure 4A) based on NH_3 gas healing method displayed an efficiency of 23.31%, with open-circuit voltage (V_{OC}) of 1.14 V, short-circuit current density (J_{SC}) of 25.36 mA/cm^2, fill factor (FF) of 80.61% and with negligible hysteresis for the device (Figure S14 and Table S1). The steady output for the best device presented a quasi-steady output of 22.32% (Figure S15). The J_{SC} of NH_3 healed $FACsPbI_3$ solar cell is comparable with the integrated J_{SC} from EQE results (24.41 mA/cm^2) in Figure 4B. The distribution histogram of 50 devices PCE at reverse scan direction is presented in Figure 4C, showing excellent reproducibility. Figure S16 is a typical cross-sectional SEM of solar cell device with 500 nm thick high dense and uniform perovskite layer. Benefiting from the high uniformity, there is no big different of the PCEs of perovskite solar cells along with increasing active areas from 0.16 cm^2 to 1.00 cm^2 (Figure 4D and Table S2). The slight decrease of FF is attributed to the increase of series resistance (Rs) from FTO substrate. A prototype PSC module (PSM) with an area of 25 cm^2 consisting 5 cells in series connection was also fabricated reaching an efficiency over 15% (Figure S17).

In Figure 4E, we also evaluated the storage stability of NH_3-$FACsPbI_3$, anti-$MAPbI_3$, anti-$FACsPbI_3$, anti-$FA_{0.9}Cs_{0.05}MA_{0.05}PbI_3$ ($FMCsPbI_3$) devices in the air with humidity around 30%. Obviously, compared to $MAPbI_3$ system, $FACsPbI_3$ system devices exhibited excellent stability in general. More specific, the device based on NH_3 gas healing method was almost no efficiency decrease under 300 days storage in the air, but the MA-rich PSCs degraded rapidly. Their phase composition, optical properties and morphologies of the 300-day-aged PSCs with different kinds of perovskite materials were studied by XRD, UV-vis and cross-section SEM (Figure S18-21). From these results, we can see that $FACsPbI_3$ devices still maintained decent cross-sectional morphology with clear grain boundaries, strong optical properties, and almost few PbI_2. However, there is a large amount of PbI_2 formed in the 300-day-aged MA-rich PSCs, resulting in the film color significantly lighter, which is because of the much lower sublimation temperature of MA than FA unit[36-37].

In closing, we have developed a low temperature non-aliphatic protic NH_3 gas post healing of FA-containing perovskite films, which provides an unprecedented capability for processing of high-quality, uniform perovskite films for high-performance photovoltaic devices and beyond. It is demonstrated that the chemical reaction between FAI and NH_3 cannot change the film composition, and in particular, the low operating temperature is vital to enable $FAPbI_3$ perovskite materials absorb enough NH_3 molecules to transform itself into a flowable intermediate state and implement the healing process. Based on this method, the $FACsPbI_3$ perovskite solar cells exhibit efficiency of 23.31%. Most importantly, this low temperature NH_3 gas post healing process is compatible with established slot die technologies and therefore opens a new direction to fabricate large scale FA-based PSCs.

Declarations

AUTHOR INFORMATION

Corresponding Author

Li Wang - Qingdao University of Science and Technology, College of Materials Science and Engineering, Qingdao, 266042, P. R. China Email: liwang718@qust.edu.cn

Guanglei Cui - Qingdao Institute of Bioenergy and Bioprocess Technology, Chinese Academy of Sciences, Qingdao 266101, P.R. China Email: cuigl@qibebt.ac.cn

Shuping Pang - Qingdao Institute of Bioenergy and Bioprocess Technology, Chinese Academy of Sciences, Qingdao 266101, P.R. China Email: pangsp@qibebt.ac.cn

ACKNOWLEDGMENT

S.P.P. thanks the supporting of the Youth Innovation Promotion Association CAS Y201944), the National Science Fund for Excellent Young Scholars (51822209), Dalian National Laboratory for Clean Energy, CAS (DICP&QIBEBT UN201705), the DNL Cooperation Fund, CAS (DNL180311). G.L.C. thanks the supporting of Major Program of Shandong Province Natural Science Foundation (ZR2018ZB0316) and the Qingdao Key Lab of Solar Energy Utilization & Energy Storage Technology.

References

(1) Kojima, A.; Teshima, K.; Shirai, Y.; Miyasaka, T., Organometal Halide Perovskites as Visible-Light Sensitizers for Photovoltaic Cells. *J. Am. Chem. Soc.* **2009,** *131* (17).

(2) Research-Cell Efficiency Records NREL, https://www.nrel.gov/pv/cell-efficiency.html (accessed: December 7, 2020).

(3) Green, M. A.; Ho-Baillie, A.; Snaith, H. J., The emergence of perovskite solar cells. *Nat. Photonics* **2014,** *8* (7), 506-514.

(4) Jeon, N. J.; Noh, J. H.; Kim, Y. C.; Yang, W. S.; Ryu, S.; Seok, S. I., Solvent engineering for high-performance inorganic-organic hybrid perovskite solar cells. *Nat. Mater.* **2014,** *13* (9), 897-903.

(5) Burschka, J.; Pellet, N.; Moon, S. J.; Humphry-Baker, R.; Gao, P.; Nazeeruddin, M. K.; Gratzel, M., Sequential deposition as a route to high-performance perovskite-sensitized solar cells. *Nature* **2013,** *499* (7458), 316-319.

(6) Jiang, Q.; Zhao, Y.; Zhang, X.; Yang, X.; Chen, Y.; Chu, Z.; Ye, Q.; Li, X.; Yin, Z.; You, J., Surface passivation of perovskite film for efficient solar cells. *Nat. Photonics* **2019**.

(7) Liu, C.; Cheng, Y. B.; Ge, Z., Understanding of perovskite crystal growth and film formation in scalable deposition processes. *Chem. Soc. Rev.* **2020,** *49* (6), 1653-1687.

(8) Li, L.; Chen, Y.; Liu, Z.; Chen, Q.; Wang, X.; Zhou, H., The Additive Coordination Effect on Hybrids Perovskite Crystallization and High-Performance Solar Cell. *Adv. Mater.* **2016,** *28* (44), 9862-9868.

(9) Yang, W. S.; Noh, J. H.; Jeon, N. J.; Kim, Y. C.; Ryu, S.; Seo, J.; Seok, S. I., High-performance photovoltaic perovskite layers fabricated through intramolecular exchange. *Science* **2015,** *348* (6240), 1234-1237.

(10) Hamill, J. C.; Schwartz, J.; Loo, Y.-L., Influence of Solvent Coordination on Hybrid Organic–Inorganic Perovskite Formation. *ACS Energy Lett.* **2017,** *3* (1), 92-97.

(11) Radicchi, E.; Mosconi, E.; Elisei, F.; Nunzi, F.; De Angelis, F., Understanding the Solution Chemistry of Lead Halide Perovskites Precursors. *ACS Appl. Energy Mater.* **2019,** *2* (5), 3400-3409.

(12) Li, Y.; Zhi, L.; Ge, G.; Zhao, Z.; Cao, X.; Chen, F.; Cui, X.; Lin, F.; Ci, L.; Sun, J.; Zhuang, D.; Wei, J., Investigation on Crystallization of $CH_3NH_3PbI_3$ Perovskite and Its Intermediate Phase from Polar Aprotic Solvents. *Cryst. Growth Des.* **2018,** *19* (2), 959-965.

(13) Fei, C. B.; Li, B.; Zhang, R.; Fu, H. Y.; Tian, J. J.; Cao, G. Z., Highly Efficient and Stable Perovskite Solar Cells Based on Monolithically Grained $CH_3NH_3PbI_3$ Film. *Adv. Energy Mater.* **2017,** *7* (9).

(14) Zhang, H.; Cheng, J.; Li, D.; Lin, F.; Mao, J.; Liang, C.; Jen, A. K.; Gratzel, M.; Choy, W. C., Toward All Room-Temperature, Solution-Processed, High-Performance Planar Perovskite Solar Cells: A New Scheme of Pyridine-Promoted Perovskite Formation. *Adv. Mater.* **2017,** *29* (13).

(15) Li, B.; Binks, D.; Cao, G.; Tian, J., Engineering Halide Perovskite Crystals through Precursor Chemistry. *Small* **2019,** *15* (47), e1903613.

(16) Lee, J. W.; Lee, D. K.; Jeong, D. N.; Park, N. G., Control of Crystal Growth toward Scalable Fabrication of Perovskite Solar Cells. *Adv. Funct. Mater.* **2018,** *29* (47), 1807047.

(17) Li, C.; Pang, S.; Xu, H.; Cui, G., Methylamine Gas Based Synthesis and Healing Process Toward Upscaling of Perovskite Solar Cells: Progress and Perspective. *Solar RRL* **2017,** *1* (9), 1700076.

(18) Zhou, Z. M.; Wang, Z. W.; Zhou, Y. Y.; Pang, S. P.; Wang, D.; Xu, H. X.; Liu, Z. H.; Padture, N. P.; Cui, G. L., Methylamine-Gas-Induced Defect-Healing Behavior of $CH_3NH_3PbI_3$ Thin Films for Perovskite Solar Cells. *Angew. Chem., Int. Ed.* **2015,** *54* (33), 9705-9709.

(19) Raga, S. R.; Jiang, Y.; Ono, L. K.; Qi, Y., Application of Methylamine Gas in Fabricating Organic-Inorganic Hybrid Perovskite Solar Cells. *Energy Technol.* **2017,** *5* (10), 1750-1761.

(20) Wang, K.; Wu, C.; Hou, Y.; Yang, D.; Li, W.; Deng, G.; Jiang, Y.; Priya, S., A Nonionic and Low-Entropic $MA(MMA)_nPbI_3$-Ink for Fast Crystallization of Perovskite Thin Films. *Joule* **2020,** *4* (3), 615-630.

(21) Yang, J.-a.; Qin, T.; Xie, L.; Liao, K.; Li, T.; Hao, F., Methylamine-induced defect-healing and cationic substitution: a new method for low-defect perovskite thin films and solar cells. *J. Mater. Chem. C* **2019,** *7* (35), 10724-10742.

(22) Liu, Q.; Zhao, Y.; Ma, Y.; Sun, X.; Ge, W.; Fang, Z.; Bai, H.; Tian, Q.; Fan, B.; Zhang, T., A mixed solvent for rapid fabrication of large-area methylammonium lead iodide layers by one-step coating at room temperature. *J. Mater. Chem. A* **2019,** *7* (31), 18275-18284.

(23) Long, M.; Zhang, T.; Chai, Y.; Ng, C. F.; Mak, T. C.; Xu, J.; Yan, K., Nonstoichiometric acid-base reaction as reliable synthetic route to highly stable $CH_3NH_3PbI_3$ perovskite film. *Nat. Commun.* **2016,** *7*, 13503.

(24) Liu, Z.; Qiu, L.; Juarez-Perez, E. J.; Hawash, Z.; Kim, T.; Jiang, Y.; Wu, Z.; Raga, S. R.; Ono, L. K.; Liu, S. F.; Qi, Y., Gas-solid reaction based over one-micrometer thick stable perovskite films for efficient solar cells and modules. *Nat. Commun.* **2018,** *9* (1), 3880.

(25) Wang, F.; Li, W.; Liu, H.; Zhu, L.; Chen, H., Cation substitution enables the complete conversion of 1D perovskites to 3D perovskites for photovoltaic application. *Nanoscale* **2019,** *11* (30), 14465-14471.

(26) Zhang, T.; Guo, N.; Li, G.; Qian, X.; Li, L.; Zhao, Y., A general non-CH_3NH_3X (X = I, Br) one-step deposition of $CH_3NH_3PbX_3$ perovskite for high performance solar cells. *J. Mater. Chem. A* **2016,** *4* (9), 3245-3248.

(27) Noel, N. K.; Habisreutinger, S. N.; Wenger, B.; Klug, M. T.; Hörantner, M. T.; Johnston, M. B.; Nicholas, R. J.; Moore, D. T.; Snaith, H. J., A low viscosity, low boiling point, clean solvent system for the rapid crystallisation of highly specular perovskite films. *Energy Environ. Sci.* **2017,** *10* (1), 145-152.

(28) Ono, L. K.; Park, N.-G.; Zhu, K.; Huang, W.; Qi, Y., Perovskite Solar Cells-Towards Commercialization. *ACS Energy Lett.* **2017,** *2* (8), 1749-1751.

(29) Chen, H.; Ye, F.; Tang, W.; He, J.; Yin, M.; Wang, Y.; Xie, F.; Bi, E.; Yang, X.; Gratzel, M.; Han, L., A solvent- and vacuum-free route to large-area perovskite films for efficient solar modules. *Nature* 2017, 550 (7674), 92-95.

(30) Juarez-Perez, E. J.; Ono, L. K.; Qi, Y., Thermal degradation of formamidinium based lead halide perovskites into sym-triazine and hydrogen cyanide observed by coupled thermogravimetry-mass spectrometry analysis. *J. Mater. Chem. A* **2019,** 7 (28), 16912-16919.

(31) Wang, X.; Fan, Y.; Wang, L.; Chen, C.; Li, Z.; Liu, R.; Meng, H.; Shao, Z.; Du, X.; Zhang, H.; Cui, G.; Pang, S., Perovskite Solution Aging: What Happened and How to Inhibit? *Chem* **2020**.

(32) Preda, N.; Mihut, L.; Baibarac, M.; Baltog, I.; Ramer, R.; Pandele, J.; Andronescu, C.; Fruth, V., Films and crystalline powder of PbI2 intercalated with ammonia and pyridine. *J. Mater. Sci.: Mater. Electron.* 2008, 20 (S1), 465-470

(33) Cataldo, F. J. E. C. B., A revision of the Gutmann donor numbers of a series of phosphoramides including TEPA. *Eur. Chem. Bull.* **2015,** *4* (1-3), 92-97.

(34) Kim, G.; Min, H.; Lee, K. S.; Lee, D. Y.; Yoon, S. M.; Seok, S. I., Impact of strain relaxation on performance of alpha-formamidinium lead iodide perovskite solar cells. *Science* 2020, 370 (6512), 108-112.

(35) Wang, Z.; Lin, Q.; Chmiel, F. P.; Sakai, N.; Herz, L. M.; Snaith, H. J., Efficient ambient-air-stable solar cells with 2D-3D heterostructured butylammonium-caesium-formamidinium lead halide perovskites. *Nat. Energy* 2017, 6, 17135.

(36) Wei, J.; Wang, Q.; Huo, J.; Gao, F.; Gan, Z.; Zhao, Q.; Li, H., Mechanisms and Suppression of Photoinduced Degradation in Perovskite Solar Cells. *Adv. Energy Mater.* 2020.

(37) Binek, A.; Hanusch, F. C.; Docampo, P.; Bein, T., Stabilization of the Trigonal High-Temperature Phase of Formamidinium Lead Iodide. *J. Phys. Chem. Lett.* 2015, 6 (7), 1249-1253.

Figures

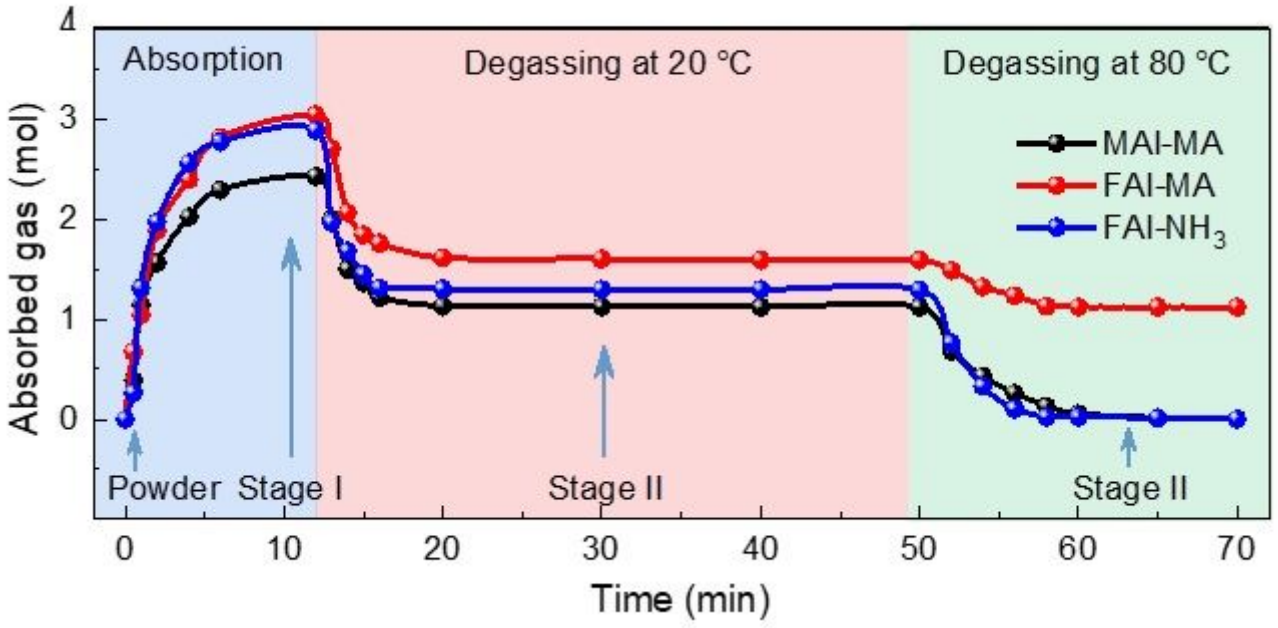

Figure 1

Absorption and Degassing Behavior of Organic Iodides MAI and FAI. The weight change of MAI/FAI in and out the MA/NH3 gas. The absorption was performed at 20 ℃, and the degassing process was carried out at 20 ℃ followed by a thermal annealing at 80 ℃.

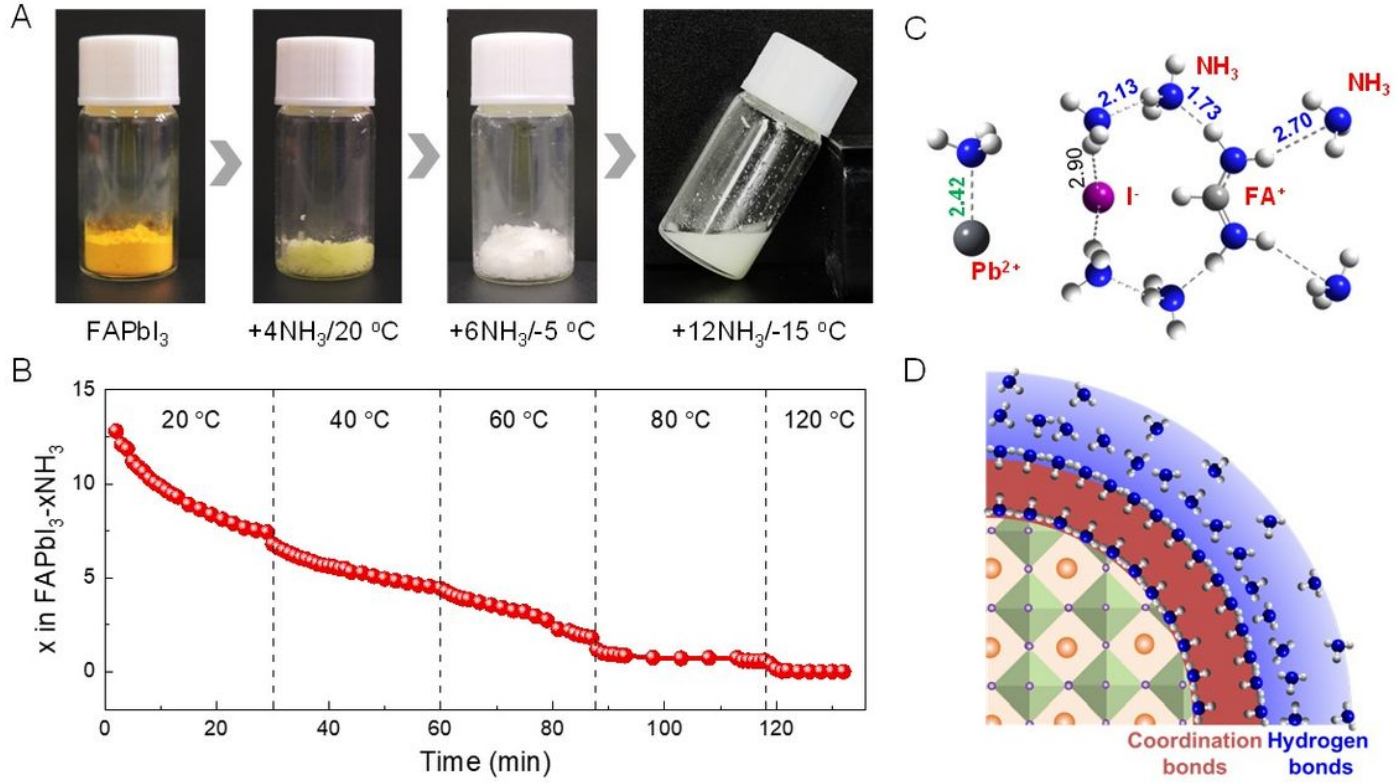

Figure 2

The Interaction between FAPbI3 and NH3 Molecules. (A) The photographs of PbI2/FAI powder in NH3 atmosphere under different temperature. (B) The calculated x value in FAPbI3·xNH3 complex in an open condition under different temperature. (C) The Pb2+-N coordination bond and hydrogen bonds formed between FAI and 6 NH3 molecules calculated with DFT. The blue values are the bond lengths (Å). (D) Schematic illustration of the coordination and hydrogen bonds in liquid FAPbI3·xNH3 complex.

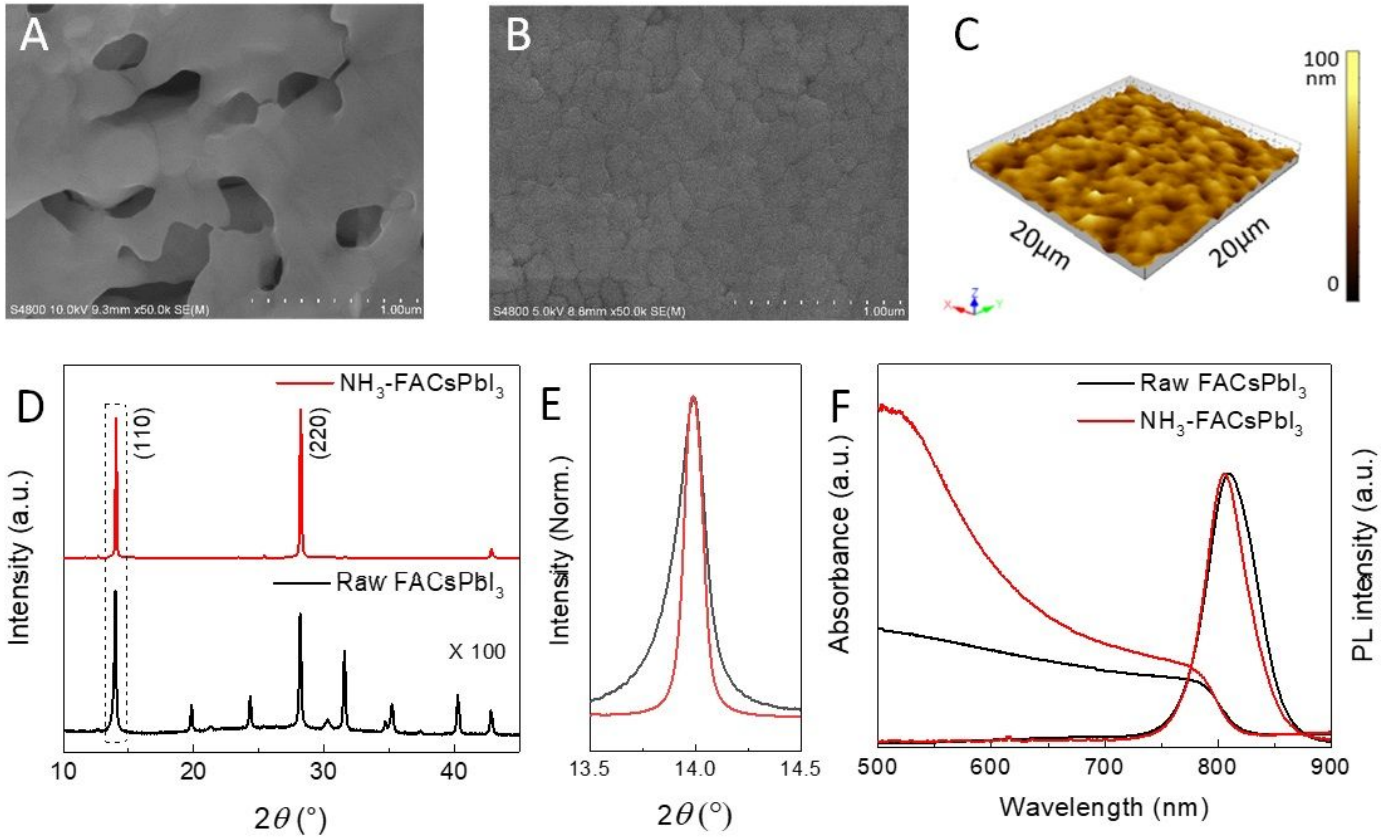

Figure 3

Properties of Perovskite Films. (A and B) SEM images of FACsPbI3 perovskite films before and after NH3 treatment. (C) AFM image of NH3 healed FACsPbI3 perovskite film with an RMS roughness of 9 nm over a 20×20 μm2 area. (D, E, and F) XRD patterns (D, E), UV-vis spectra and steady PL spectra (F) of FACsPbI3 thin films before and after NH3 treatment, respectively.

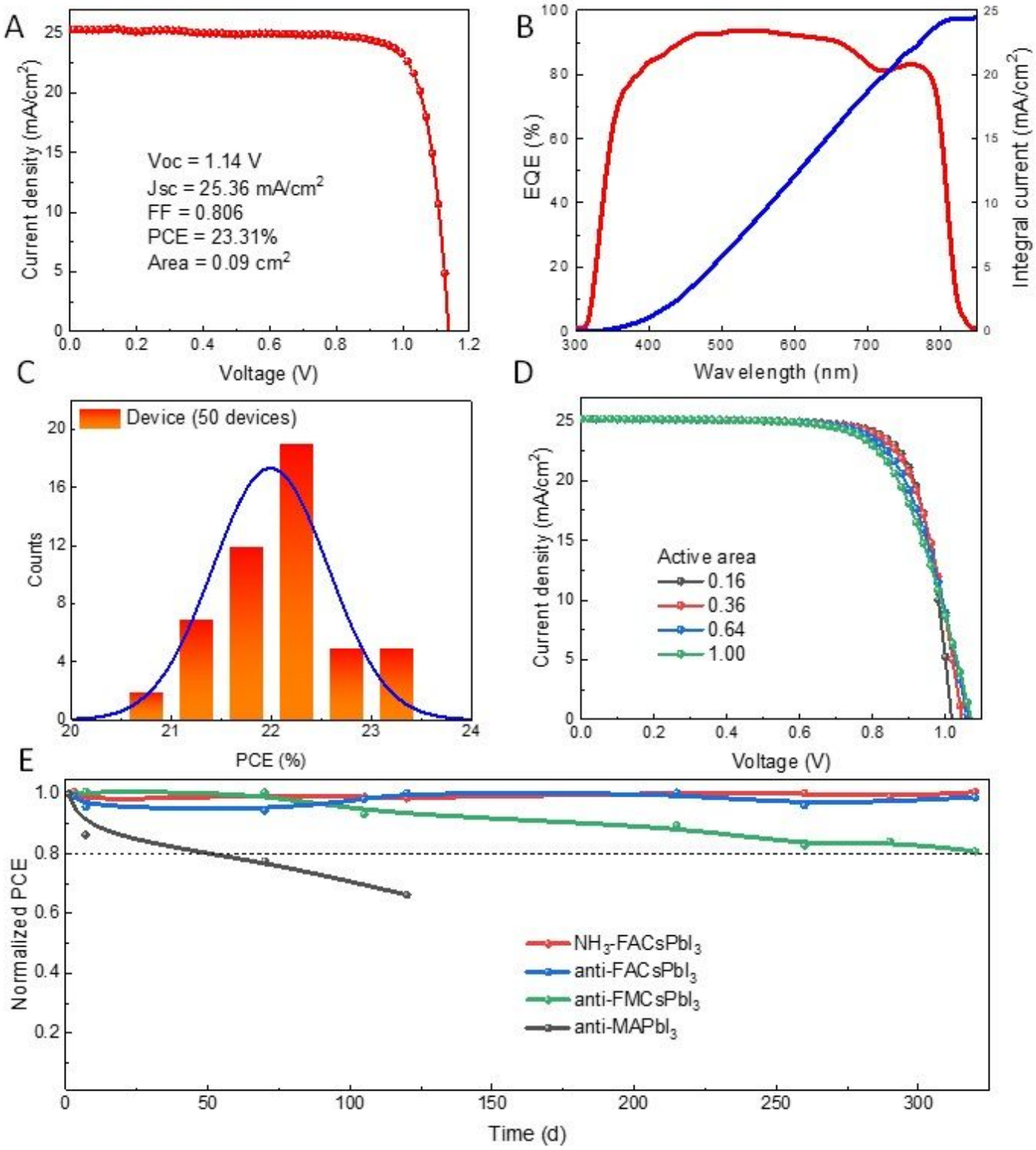

Figure 4

Solar Cell Device Performance. (A) The best device we achieved through the NH3 gas healing method. (B) EQE of the best device, the integrated JSC from the EQE is 24.41 mA/cm2. (C) Histogram of the power conversion efficiency determined for 50 PSC devices. (D) J-V characteristics of NH3 healed FACsPbI3 perovskite solar cells measured with various active areas. (E) Results of humidity stability tests on the

unencapsulated NH3-FACsPbI3, anti-FACsPbI3, anti-FA0.9MA0.5Cs0.5PbI3 and anti-MAPbI3 devices under 30% relative humidity at room temperature.

Supplementary Files

This is a list of supplementary files associated with this preprint. Click to download.

- Schemes.pdf
- Supporting.docx
- TOC.jpg